C. R. Mecanique 340 (2012) 471–476

Contents lists available at SciVerse ScienceDirect

Comptes Rendus Mecanique

www.sciencedirect.com

Analytical and innovative solutions for heat transfer problems involving phase change and interfaces

Solid–liquid phase change driven by internal heat generation

John Crepeau [a,*], Ali S. Siahpush [b]

[a] Department of Mechanical Engineering, PO Box 440902, University of Idaho, Moscow, ID 83844-0902, USA
[b] Idaho National Laboratory, PO Box 1625, MS 3760, Idaho Falls, ID 83415-3760, USA

ARTICLE INFO

Article history:
Available online 3 May 2012

Keywords:
Stefan Problem
Internal heat generation
Scale analysis

ABSTRACT

This article presents results of solid–liquid phase change, the Stefan Problem, where melting is driven internal heat generation, in a cylindrical geometry. The comparison between a quasi-static analytical solution for Stefan numbers less than one and numerical solutions shows good agreement. The computational results of phase change with internal heat generation show how convection cells form in the liquid region. A scale analysis of the same problem shows four distinct regions of the melting process.

1. Introduction

The first published solution to the solid–liquid phase change problem was given by Joseph Stefan in 1889 [1], and has been known as the Stefan Problem since the pioneering monograph by Rubinstein [2]. Reviews of the state-of-the-art work on the Stefan Problem have also been published [3,4]. Due to the phase change along the interface, convection and flow instabilities can form [5]. Phase change by internal heat generation has numerous applications, including geophysics and materials processing, but most work has been done in nuclear energy. Simple transient models of reactor pins [6], successive approximation methods of flow in a reactor plug [7], numerical studies in a heat generating slab [8], and the enthalpy method to model the mushy zone [9] have been studied. The Nusselt number and other heat transfer characteristics of flows with internal heat generation in tubes [10] have been determined.

The governing mass, momentum and energy equations in cylindrical coordinates, with no change in the circumferential direction, are given by [11],

$$\frac{\partial u}{\partial r}+\frac{\partial w}{\partial z}=0 \tag{1}$$

$$u\frac{\partial w}{\partial r}+w\frac{\partial w}{\partial z}=-g\beta\Delta T+\nu\left(\frac{\partial^2 w}{\partial r^2}+\frac{1}{r}\frac{\partial w}{\partial r}+\frac{\partial^2 w}{\partial z^2}\right) \tag{2}$$

$$\frac{\partial T}{\partial t}+u\frac{\partial T}{\partial r}+w\frac{\partial T}{\partial z}=\frac{\dot{q}}{\rho c_p}+\alpha\left(\frac{\partial^2 T}{\partial r^2}+\frac{1}{r}\frac{\partial T}{\partial r}+\frac{\partial^2 T}{\partial z^2}\right) \tag{3}$$

In Eq. (2), the Boussinesq approximation is used to model the buoyancy term. The geometry of the problem is shown in Fig. 1.

* Corresponding author.
E-mail addresses: crepeau@uidaho.edu (J. Crepeau), ali.siahpush@inl.gov (A.S. Siahpush).

1631-0721/$ – see front matter
doi:10.1016/j.crme.2012.03.004

Nomenclature

c_p	specific heat, kJ/kg K	t	time, s
Δh_f	latent heat of fusion, kJ/kg	T	temperature, K
g	gravitational acceleration, m/s^2	u, w	velocities, m/s
H	cylinder height, m	α	thermal diffusivity, m^2/s
k	thermal conductivity, W/mK	β	thermal expansion coefficient, K^{-1}
$\dot{q}$	volumetric heat generation, W/m^3	θ	nondimensional temperature
Q	nondimensional heat generation	μ	viscosity, kg m/s^2
r, z	radial coordinates, m	ρ	density, kg/m^3
r_0	radius of cylinder, m	τ	nondimensional time
s	distance to phase change front, m	ξ	nondimensional radius

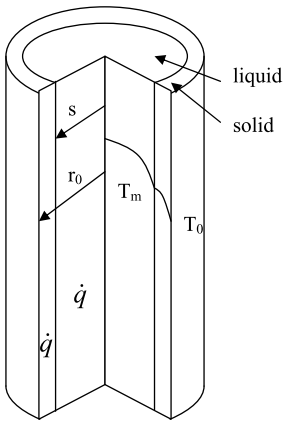

Fig. 1. Schematic diagram of phase change in a cylinder with volumetric heat generation.

2. Comparison of quasi-static and numerical solutions

We begin by assuming that the phase change occurred at a single fusion temperature (i.e., a pure material), that the internal heat generation was constant, uniform, and equal in both the solid and liquid phases. Also, for this analysis, there was no convection heat transfer in the liquid, so that heat transferred solely by conduction. The cylinder was infinitely long so end effects were neglected. At r_0, the temperature is held constant at T_0, and at the phase change interface the temperature is the melting, T_m, was constant. The fusion temperature is greater than the surface temperature, so a solid layer forms along the wall.

Under these conditions, the energy equation (Eq. (3)) for both the solid and liquid phases reduces to

$$\frac{1}{r}\frac{\partial}{\partial r}\left(kr\frac{\partial T}{\partial r}\right)+\dot{q}=\rho c_p\frac{\partial T}{\partial t} \tag{4}$$

Along the phase change front, the interface equation is given by [12],

$$k_{liq}\frac{\partial T_{liq}}{\partial r}\bigg|_{r=s}+\rho_{sol}\Delta h_f\frac{\mathrm{d}s}{\mathrm{d}t}=k_{sol}\frac{\partial T_{sol}}{\partial r}\bigg|_{r=s} \tag{5}$$

Integrating Eq. (4) in its quasi-static form ($\partial T/\partial t=0$) produces temperature gradients in both the solid and liquid phases,

$$\frac{\mathrm{d}T_{liq}}{\mathrm{d}r}\bigg|_{r=s}=-\frac{\dot{q}s}{2k_{liq}} \tag{6}$$

$$\frac{\mathrm{d}T_{sol}}{\mathrm{d}r}\bigg|_{r=s}=-\frac{\dot{q}s}{2k_{sol}}+\frac{(s^2-r_0^2)\dot{q}+4k_{sol}(T_m-T_0)}{4k_{sol}s(\ln s-\ln r_0)} \tag{7}$$

Substituting Eqs. (6) and (7) into the interface equation (Eq. (5)) produces a relation governing motion of the phase change front,

$$\rho_{sol}\Delta h_f\frac{\mathrm{d}s}{\mathrm{d}t}=\frac{(s^2-r_0^2)\dot{q}+4k_{sol}(T_m-T_0)}{4s(\ln s-\ln r_0)} \tag{8}$$

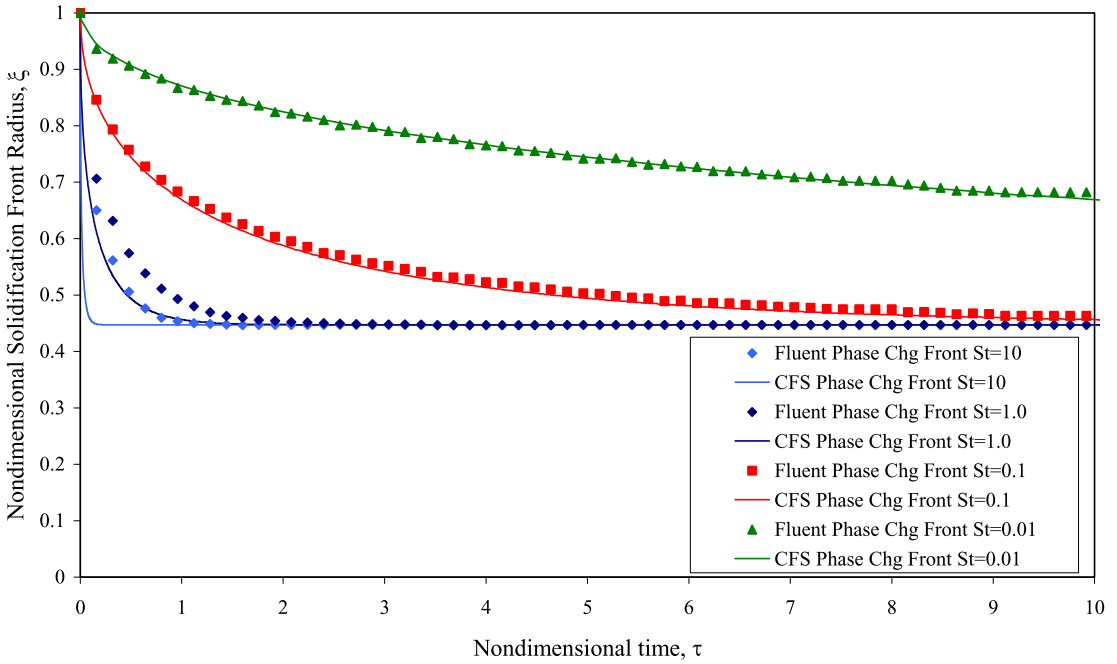

Fig. 2. Comparison of computational and analytical solutions for $Q = 5.0$, and Stefan numbers both in and out of the range of validity of the quasi-static method in a cylindrical geometry for a constant surface temperature during solidification.

Nondimensionalizing Eq. (8) with the variables,

$$\xi = \frac{s}{r_0}, \qquad \tau = \frac{\alpha t}{r_0^2}, \qquad Q = \frac{\dot{q} r_0^2}{k(T_m - T_0)}, \qquad \theta = \frac{T - T_0}{T_m - T_0}, \qquad St = \frac{c_p(T_m - T_0)}{\Delta h_f} \tag{9}$$

where St is the Stefan number, the nondimensional interface relation becomes [13],

$$\frac{1}{St}\frac{\mathrm{d}\xi}{\mathrm{d}\tau} = \frac{4 + (\xi^2 - 1)Q}{4\xi \ln \xi} \tag{10}$$

Eq. (10) can then be solved for the nondimensional distance to the phase change front, ξ.

To verify the accuracy of the quasi-static solutions, a computational model using the code FLUENT® was developed. The computational method used an energy equation solution technique to solve for solidification/melting that is based on the enthalpy–porosity method [14].

Eq. (10) was then solved and compared to the computational solutions. Fig. 2 shows results for the nondimensional internal heat generation of $Q = 5$ over four decades of Stefan numbers both in and out of the range of validity of the quasi-static method. The curves show excellent agreement between the two methods for $St = 0.1$ and 0.01, where the quasi-static approximation used in the analytical solution is valid. Outside of the range where the quasi-static approximation is valid, $St = 1.0$ and 10.0, the analytic solutions reach steady state more quickly than the computational results. This is because the elimination of the time-dependent term from which the temperature gradients are calculated forces the resultant temperature profiles to reach the steady-state values more rapidly than the profiles given in the computational results. However, both reach the same value of the steady-state phase change front location. Fig. 3 is similar to Fig. 2 except that Eq. (10) is plotted for $St = 0.1$ and a range of Q. The agreement is very good between the analytical and computational solutions for these curves which are valid under the quasi-static approximation.

3. Phase change and convection in the melt driven by VEG

To determine the effect that convection has on the phase change process, a numerical study was performed. Since the convection heat transfer was driven by the internal heat generation and not a simple temperature difference, a modified version of the Rayleigh number was used. After Tritton and Zarraga [15] and Roberts [16], we used the definition

$$Ra = \frac{\rho g \beta \dot{q} D^5}{\mu \alpha k} \tag{11}$$

Fig. 4 [17] shows a single snapshot of system using the Rayleigh number defined in Eq. (11), where $Ra = 10^6$, $Q = 5.0$, and $St = 0.1$. The solid phase is in blue along the outer portion of the cylinder, red corresponds to the liquid phase and the

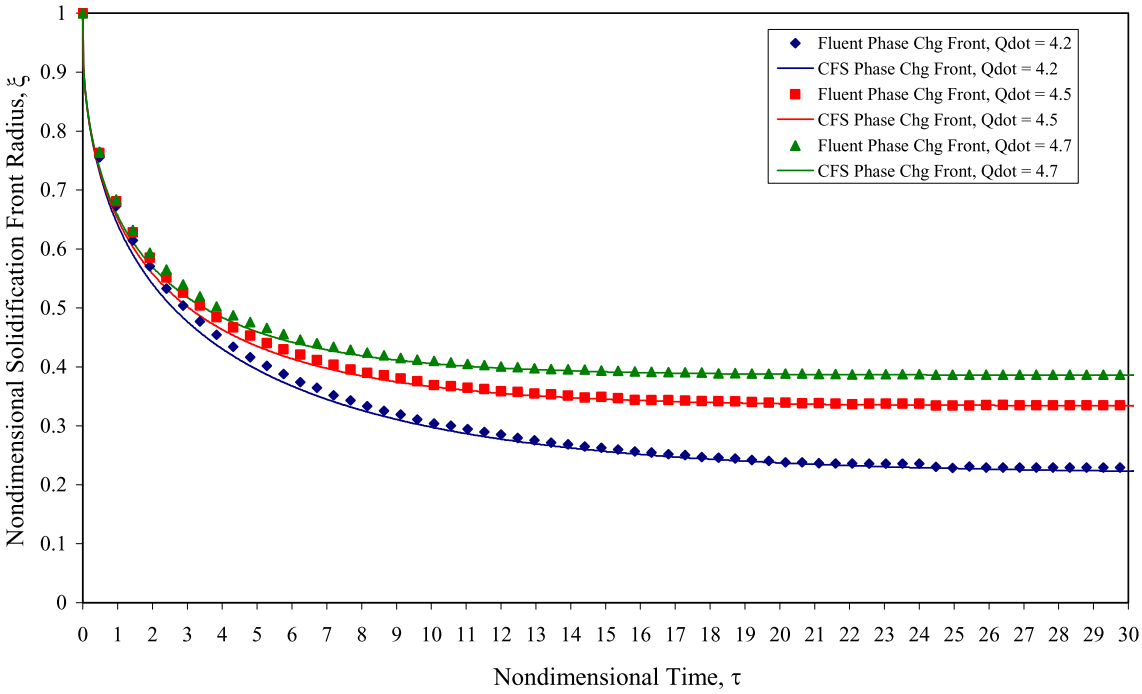

Fig. 3. Comparison of computational and analytical solutions for $St = 0.1$ and various values of Q in a cylindrical geometry for constant surface temperature during solidification.

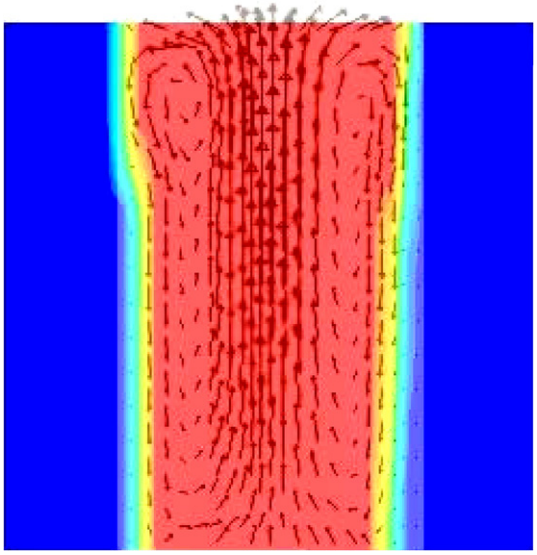

Fig. 4. Movement of the solid–liquid phase change front and velocity vectors in the liquid region during solidification at $Ra = 10^6$, $Q = 5.0$ and $St = 0.1$ [16].

intermediate colors represent the mushy zone. Velocity vectors are superimposed to give a quantitative representation for the motion of the fluid. A small recirculation zone forms at the top of the cylinder, melting more material at the top than at the bottom. At larger values of *Ra*, the recirculation zone becomes more pronounced.

4. Scale analysis

This section gives a brief overview using scale analysis to study the phase change process driven by internal heat generation in a cylinder. A more in-depth study was presented previously [18]. Scale analysis has been extensively used by Bejan [19,20]. The phase change process can be divided into four regimes. We initially considered the material within the cylinder to be completely solid.

Regime A is when a thin layer of liquid forms along the centerline. There is no convection in the liquid, and since melting has just begun, the temperature of the liquid is just above the melting point. Since the liquid temperature is constant, Eq. (5) becomes

$$\rho_s \Delta h_f \frac{\mathrm{d}s}{\mathrm{d}t} = k_s \frac{\mathrm{d}T_s}{\mathrm{d}r} \tag{12}$$

Substituting Eq. (12) into Eq. (7) and rearranging give

$$\frac{\mathrm{d}s}{\mathrm{d}t} = -\frac{\dot{q}s}{2\rho_s \Delta h_f} + \frac{(s^2 - r_0^2)\dot{q}}{4s\ln(s/r_0)\rho_s \Delta h_f} + \frac{\alpha St_s}{s\ln(s/r_0)} \tag{13}$$

Since the diameter of the melted region is small compared to the radius, $s \ll r_0$, we find

$$t_A \sim \frac{\rho_s \Delta h_f}{\dot{q}} \tag{14}$$

and at this time, Regime A ends. Typically this time is very short.

In Regime B, the liquid layer grows, but the temperature is no longer constant throughout and no convection cells have yet formed. In this regime, Eq. (5) scales like

$$\frac{s^2}{t} \sim \frac{r_0^2 \dot{q}}{\rho_s \Delta h_f \ln(s/r_0)}, \qquad \frac{\alpha St_l}{\ln(s/r_0)} \tag{15}$$

For small Stefan numbers, we have

$$t_B \sim \frac{\rho_s \Delta h_f}{\dot{q}} \frac{s^2}{r_0^2} \tag{16}$$

Regime C begins when convection starts in the liquid portion of the melt. Experimental evidence [21] shows that convection in the liquid begins along the top portion of the cylinder and along the bottom of the cylinder, heat transfers by conduction. The governing equations (Eqs. (1)–(3)) scale like

$$\begin{aligned} &\frac{u}{s} \sim \frac{w}{H} \\ &\frac{w^2}{H} \sim \beta g \Delta T_l, \qquad \nu \frac{w}{s^2} \\ &\frac{w}{H}\Delta T_l, \qquad \frac{\dot{q}}{\rho c_p} \sim \alpha \frac{\Delta T_l}{s^2} \end{aligned} \tag{17}$$

After inserting these scaling terms into Eq. (5) and reducing, we find

$$t_C \sim \frac{\rho \Delta h_f}{\dot{q}} \left[\left(\frac{1}{Ra_H} \right)^{1/6} \frac{H}{r_0} \right]^2 \tag{18}$$

where H is the height of the cylinder, and the Rayleigh number is defined in Eq. (11).

In the final stage of the phase change process, Regime D, the convection cell takes up the complete length of the cylinder. Here, the governing equations scale like

$$\begin{aligned} &\frac{w}{H}\Delta T_l \sim \frac{\dot{q}}{\rho_l c_{p,l}} \\ &\beta g \Delta T_l \sim \nu_l \frac{w}{s^2} \end{aligned} \tag{19}$$

Scaling Eq. (5) by the terms in Eq. (19) yields a differential equation,

$$\frac{1}{2} Nu_D \tilde{T}_l + \frac{1}{St_l} \frac{\mathrm{d}\tilde{s}}{\mathrm{d}\tau} = -\frac{\mathrm{d}T_s}{\mathrm{d}\tilde{r}_s} \tag{20}$$

where,

$$\tilde{s} = \frac{s}{r_0}, \qquad \tau = \frac{\alpha_s}{r_0^2} t, \qquad \tilde{r}_s = \frac{r_s}{r_0}, \qquad \tilde{T}_s = \frac{T_m - T_s}{T_m - T_0}, \qquad \tilde{T}_l = \frac{T_{CL} - T_s}{T_m - T_0}, \qquad Nu_D = \frac{hD}{k} \tag{21}$$

Eq. (20) can then be solved numerically to give the distance to the phase front, s, in terms of time.

5. Conclusions

Comparison of the quasi-static and numerical solutions of the Stefan Problem shows good agreement when $St \ll 1$, which is when the quasi-static solution is valid. The scale analysis shows the existence of four separate regimes, each with an appropriate time scale associated with the process. The scale analysis gives a straightforward way to model the phase change process driven by internal heat generation.

References

[1] J. Stefan, Über die Theorie der Eisbildung, insbesondere über die Eisbildung im Polarmeere, Sitzungsberichte der k.k. Akademie der Wissenschaften in Wien, Mathematische–Naturwissenschaften, Abteilung II (98), 1889, pp. 965–983.
[2] L.I. Rubinstein, The Stefan Problem, AMS Publications, Providence, RI, 1971.
[3] R. Viskanta, Heat transfer during melting and solidification of metals, J. Heat Transfer 110 (1988) 1205–1219.
[4] L.S. Yao, J. Prusa, Melting and freezing, Adv. Heat Transfer 19 (1989) 1–95.
[5] E.A. Semma, M. El Ganaoui, A. Cheddadi, P. Bontoux, Étude numérique des instabilités de la phase fluide et de l'interface de solidification en croissance dirigée horizontale, C. R. Mecanique 331 (2003) 631–639.
[6] W.L. Chen, M. Ishii, M.A. Grolmes, Simple heat conduction model with phase change for reactor fuel pin, Nuclear Sci. Eng. 60 (1976) 452–460.
[7] M. El-Genk, A.W. Cronenburg, An assessment of fuel freezing and drainage phenomena in a reactor shield plug following a core disruptive accident, Nuclear Eng. Design 47 (1978) 195–225.
[8] F.B. Cheung, T.C. Chawla, D.R. Pedersen, The effects of heat generation and wall interaction on freezing and melting in a finite slab, Int. J. Heat Mass Transfer 27 (1984) 29–37.
[9] S.H. Chan, K.Y. Hsu, Generalized phase change model for melting and solidification with internal heat generation, J. Thermophysics 1 (1987) 171–174.
[10] Y. Kikuchi, Y. Shigemasa, Liquid solidification in laminar tube flow with internal heat sources, Nuclear Eng. Design 75 (1982) 73–80.
[11] F. Incropera, D. DeWitt, Fundamentals of Heat and Mass Transfer, 4th ed., Wiley, New York, 2002.
[12] D. Poulikakos, Conduction Heat Transfer, Prentice Hall, Englewood Cliffs, 1994.
[13] J. Crepeau, A. Siahpush, Approximate solutions to the Stefan problem with internal heat generation, Heat Mass Transfer 44 (2008) 787–794.
[14] R. Voller, C. Prakash, A fixed-grid numerical modeling methodology for convection–diffusion mushy region phase-change problems, Int. J. Heat Mass Transfer 30 (1987) 1709–1720.
[15] D.J. Tritton, M.N. Zarraga, Convection in horizontal layers with internal heat generation. Experiments, J. Fluid Mechanics 30 (1967) 21–31.
[16] P.H. Roberts, Convection in horizontal layers with internal heat generation. Theory, J. Fluid Mechanics 30 (1967) 33–49.
[17] J.C. Crepeau, A. Siahpush, B. Spotten, On the Stefan problem with volumetric energy generation, Heat Mass Transfer 46 (2009) 119–128.
[18] J.C. Crepeau, A. Siahpush, Scale analysis of convective melting with internal heat generation, in: Proc. ASME/JSME 8th Thermal Engineering Joint Conference, paper #44162, Honolulu, Hawaii, 2011.
[19] A. Bejan, Convection Heat Transfer, 3rd ed., Wiley, New York, 2004.
[20] Z. Zhang, A. Bejan, The problem of time-dependent natural convection melting with conduction in the solid, Int. J. Heat Mass Transfer 32 (1989) 2447–2457.
[21] A. Siahpush, J. O'Brien, J. Crepeau, Phase change heat transfer enhancement using copper porous foam, J. Heat Transfer 130 (2008) 082301, 11 pages.